RESEARCH PAPER

Improving physicochemical, mechanical, and biological properties of a porous polyvinyl alcohol/chitosan matrix via modification with magnesium and silicon agents

Nima Vakili[1], Azadeh Asefnejad[1]*, Mohammad Mohammadi[1], Hessam Rezaei[1], Amirsalar Khandan[2]

[1]Department of Biomedical Engineering, Science and Research Branch, Islamic Azad University, Tehran, Iran
[2]Dental Research Center, Department of Endodontics, Dental Research Institute, School of Dentistry, Isfahan University of Medical Sciences, Isfahan, Iran

ABSTRACT

Objective(s): Biocomposite scaffolds made from polymers and bioactive materials can provide the necessary bioactivity and mechanical properties for bone tissue engineering.

Materials and Methods: In this study, we aimed to evaluate the properties of a novel composite scaffold made from a combination of chitosan, PVA, $MgCl_2$, and GPTMS as a crosslinking agent. Scanning Electron Microscopy (SEM) and Fourier-Transform Infrared Spectroscopy (FTIR) analysis characterized the prepared composite scaffold. The composite scaffolds' mechanical properties, bioactivity, biocompatibility, swelling, and degradation were also investigated.

Results: Significant improvements in the mechanical properties were observed in the modified composite compared to those seen in the scaffold without $MgCl_2$. With an increase in $MgCl_2$ content, the scaffold's degradation and porosity increased, while its swelling capacity decreased. Bioactivity was also enhanced in the composite following the further addition of $MgCl_2$.

Conclusion: In vitro tests for cytotoxicity and MG-63 cell proliferation showed that the composite scaffolds were non-cytotoxic, resulting in better cell adherence and growth on the surface of these scaffolds.

Keywords: *PVA-chitosan Scaffolds, Magnesium chloride, GPTMS, Osseointegrability, Dental materials*

How to cite this article

Vakili N, Asefnejad A, Mohammadi M, Rezaei H, Khandan A. Improved physicochemical, mechanical, and biological properties of a porous polyvinyl alcohol/chitosan matrix via modification with magnesium and silicon agents. Nanomed J. 2025; 12(3):507-517. DOI: 10.22038/NMJ.2025.79321.1951

INTRODUCTION

Each year, an increasing number of individuals experience bone defects due to diseases, tumors, biochemical disorders, and infections. Traditional biological procedures for bone grafting, including autografts, allografts, and non-degradable materials, have been employed to address these issues [1-3]. However, significant drawbacks—such as the limited availability of donors, risks of disease transmission, and potential immune rejection—have restricted their clinical use [4-5]. Consequently, tissue engineering offers a viable solution by utilizing biocompatible, biodegradable materials to facilitate tissue regeneration. Various inorganic materials, including metals and ceramics, have been explored as implants to promote bone regeneration. Nevertheless, these biomaterials often exhibit insufficient regenerative capabilities due to limitations related to immunogenicity, lack of resorption, non-degradability, and inadequate interconnective porosity [6-9]. Bone tissue engineering provides biopolymeric scaffolds as practical solutions for bone tissue regeneration. Among synthetic polymers, chitosan—extracted from crustacean shells and the cell walls of certain fungi—has been widely utilized in bone tissue engineering applications. Unlike many synthetic polymers, chitosan possesses a hydrophilic surface that enhances cell adhesion and proliferation, and its degradation products are non-toxic. Chitosan promotes the attachment and proliferation of osteoblasts, facilitating the formation of a mineralized bone matrix, making it a promising material for bone scaffolds [10-14]. However, chitosan alone lacks the mechanical strength necessary to support cell growth; thus, it can be combined with other biomaterials, such as additional polymers, to create composite scaffolds

*Corresponding author(s) Email: asefnejad@srbiau.ac.ir;
Note. This manuscript was submitted on April 14, 2024; approved on December 09, 2024

with improved mechanical and biological properties [15-17]. Another biodegradable polymer frequently employed in tissue engineering is poly(vinyl alcohol) (PVA), a semi-crystalline hydrophilic polymer known for its good chemical stability [18-19]. PVA is highly biocompatible, biodegradable, and non-toxic, which has led to its application as a biopolymer in bone tissue engineering. Research has indicated that the combination of chitosan and PVA yields scaffolds with desirable mechanical and chemical properties [20-22].

The properties necessary for scaffolds used in bone tissue engineering extend beyond promoting cell adhesion and proliferation; they must also exhibit biocompatibility, biodegradability, and high mechanical strength. Research indicates that glycidoxypropyl trimethoxy silane (GPTMS) can stimulate apatite nucleation and growth in physiological environments while being cytocompatible, thus supporting MC3T3-E1 cell culture. The capability of apatite deposition enhances the fixation of scaffolds to tissue defects by forming direct bonds. GPTMS, a silane-coupling agent characterized by its epoxy and methoxysilane groups, is non-toxic and capable of creating a networked structure, unlike various cross-linking agents such as epoxy compounds and aldehydes, which are often highly cytotoxic and can impair the biocompatibility of polymers [19-22]. Addressing challenges in healing bone defects and fractures, incorporating growth factors into implantable scaffolds has been recognized as a promising strategy. Among these, bone morphogenetic protein-2 (BMP-2), derived from transforming growth factor-β (TGF-β), is known for its potent osteogenic properties. However, the clinical application of BMP-2 is limited due to its short biological half-life, rapid local clearance, potential side effects such as ectopic ossification, and high treatment costs [23-25]. Incorporating bioactive ions such as Si, Mg, Ca, Zn, and Sr has emerged as an effective method to enhance the bioactivity of biomaterials. Magnesium, the second most abundant intracellular divalent cation associated with biological apatite, is crucial in calcification and bone biomineralization [25-28]. In this respect, we aimed to study the effect of Mg on the new composition of the pore structure, water uptake, mechanical properties, bioactivity, and cytocompatibility of the porous chitosan-PVA-GPTMS-$MgCl_2$ scaffolds, which were prepared using the freeze-drying technique. The primary objective of this study was to develop and characterize novel porous composite scaffolds composed of chitosan, polyvinyl alcohol (PVA), glycidyloxypropyltrimethoxysilane (GPTMS), and magnesium chloride ($MgCl_2$) for potential application in bone tissue engineering. Incorporating $MgCl_2$ into the chitosan-PVA-GPTMS matrix is a unique approach that has not been extensively explored in the literature. The researchers aimed to investigate the effect of $MgCl_2$ on the composite scaffolds' physicochemical, mechanical, and biological properties, which could potentially enhance their suitability for bone regeneration. The study provides valuable insights into developing biocomposite scaffolds with improved mechanical properties, bioactivity, and biodegradation characteristics by adding $MgCl_2$. The in vitro evaluation of the scaffolds' biocompatibility and their ability to support the proliferation of MG-63 osteoblast cells further demonstrates their potential for bone tissue engineering applications. The results of this research contribute to the ongoing efforts to design and optimize advanced biomaterial-based scaffolds for effective bone regeneration.

MATERIALS AND METHODS

Preparation of hybrid composite (Polymer/GPTMS/MgCl2)

Poly(vinyl alcohol) (PVA) with a molecular weight of 72,000 g/mol, 3-glycidoxypropyltrimethoxysilane (GPTMS), and acetic acid were obtained from Merck, while chitosan [poly(β-(1-4)-2-amino-2-deoxy-D-glucopyranose)] was sourced from Sigma-Aldrich. SAMCHUN supplied magnesium chloride ($MgCl_2$). A 3% (w/v) solution of chitosan/PVA in a 50:50 weight ratio was prepared using a 2% (v/v) acetic acid solvent. GPTMS and $MgCl_2$ were subsequently incorporated into the polymeric solution in varying ratios of Polymer/GPTMS/$MgCl_2$ (5:5:0.5, 5:5:1, 5:5:2), resulting in the compositions listed in Table 1. The samples were coded according to the precursor solution compositions, as shown in Table 1.

Table 1. Notation of different freeze dried scaffolds studied in this work

Codes	Composition (Weight ratio)	$MgCl_2$: Polymers (Weight ratio)	Freezing temperature (°C)	Polymer: GPTMS (molar ratio)
5C5P0.5M	Chitosan: PVA 50:50	0.5:5	-20	1:1
5C5P1M	Chitosan: PVA 50:50	1:5	-20	1:1
5C5P2M	Chitosan: PVA 50:50	2:5	-20	1:1

All polymer solutions were then poured into cylindrical molds with a diameter of 1 cm and placed in a freezer to solidify overnight. Following this, the solidified solutions were subjected to freeze-drying at -58°C and a pressure of 0.5 bar for 48 hours to completely remove the solvent and water phase.

Structure characterization

A scanning electron microscope (SEM, STEREOSCAN S 360-Leica, UK) was employed to examine the morphology of the 3D scaffold. Image analysis software was used to quantify pore sizes. For each procedure, a minimum of twenty pores were selected from three distinct sample areas. The percentage of total porosity (P) was calculated by comparing the density of the scaffold to the initial density of the powder, as shown in Equation 1.

$$\boldsymbol{P = 1 - \frac{\rho_{scaffold}}{\rho_{solid}}} \qquad \textbf{Eq.1}$$

A minimum of 5 samples were analyzed until the correct standard deviation of the percentage of porosity was obtained. The PVA, chitosan, GPTMS, $MgCl_2$, and grafted Polymer/GPTMS/$MgCl_2$ 3D scaffolds were analyzed by FT-IR (FTIR, Nicolet Is10, USA) over a range of 4000–400 cm^{-1}.

Mechanical testing

The compressive behavior of Polymer/ GPTMS/ $MgCl_2$ hybrid scaffolds with varying compositions was evaluated using a mechanical testing system (SANTAM, STM 20, Iran) at a compression rate of 0.5 mm/min. Five samples from each composition (n = 5) were tested to determine the average value and standard deviation.

Absorption and biodegradation test

The swelling and dissolution behaviors of the scaffolds were assessed using phosphate-buffered saline (PBS) at pH 7.4 (Sigma–Aldrich). The PBS solution was prepared according to previously established protocols. The degree of swelling was measured at 2, 4, 6, and 24 hours, while the dissolution degree was evaluated after 1, 2, 3, and 4 weeks. The swelling percentage was calculated as follows:

$$\boldsymbol{\Delta W_s = \left(\frac{w_s - w_o}{w_o}\right) \times 100} \qquad \textbf{Eq.2}$$

Where W_0 and W_S are the sample weights before and after swelling, respectively.

After drying at 37°C for 48 h in an oven, samples were weighed again, and the degradation percentage was calculated as:

$$\boldsymbol{\Delta W_d = \left(\frac{w_s - w_d}{w_o}\right) \times 100} \qquad \textbf{Eq.3}$$

Where W_d is the dried sample weight. Five samples were measured for each interval, and the result was shown as an average value ± standard deviation.

In vitro bioactivity assays

The in vitro bioactivity of the composite scaffold (5C5P1M) was studied by soaking samples in Simulated Body Fluid (SBF) solution. The SBF was prepared as described by Kokubo et al., and the scaffolds were immersed in it at 37°C for 3, 7, and 14 days. Scanning Electron Microscopy (SEM) and Fourier-Transform Infrared Spectroscopy (FTIR) were used to evaluate apatite formation.

Characterization and in vitro biocompatibility
MTT assay

To conduct the MTT assay, MG-63 cells were cultured on the scaffolds for 3 and 5 days, and their proliferation rates were compared with those of cultured osteoblasts. Five samples were prepared for the 5C5P1M scaffold. MG-63 osteoblast cells were maintained in DMEM medium supplemented with 10% fetal bovine serum, 1% penicillin–streptomycin, and 1.2% glutamine. The cultures were incubated at 37°C in a humidified atmosphere containing 5% CO_2. Once the cells reached 80% confluence, they were trypsinized using 0.25% trypsin with 1 mM EDTA. Cell viability was assessed using the MTT (3-[4,5-dimethylthiazol-2-yl]-2,5-diphenyltetrazolium bromide; Thiazolyl blue) assay. Before the MTT assay, the 5C5P1M scaffolds were sterilized using high-pressure steam for 15 minutes and placed into wells of a 24-well culture plate. The samples were then incubated in 1 mL of DMEM medium at 37°C for 24 hours. After this incubation, the membranes were removed, and the resulting extracts were collected. MG-63 cells were seeded in a 96-well plate at a density of 10^3 cells per well. Following an additional 24-hour incubation, the culture medium was replaced with the previously prepared extraction medium, and the cells were incubated for another 24 hours. Subsequently, 100 µL of MTT solution was added to each well. After a 3-hour incubation at 37°C, 200 µL of dimethyl sulfoxide was added to dissolve the formazan crystals. The resulting solution was mixed thoroughly for 10 minutes using a shaker. The optical density of the formazan solution was measured using an ELISA reader at 570 nm.

SEM observation of cell culture and adhesion

Cells were seeded into fresh culture medium (control) under the same seeding conditions for reference. The sterilized scaffolds were washed

three times with sterile phosphate-buffered saline (PBS) and transferred to individual 24-well tissue culture plates. Aliquots (1 mL) of osteoblast MG-63 suspension (1.5×10^4 cells/mL) were seeded onto the sample membranes. After 48 hours of culture, cellular constructs were harvested, rinsed twice with PBS to remove non-adherent cells, and then fixed with 3.0% glutaraldehyde at 4°C for 4 hours. The samples were subsequently dehydrated through a series of graded ethanol solutions and air-dried overnight. Finally, the dried samples were sputter-coated with gold to observe cell morphology on the surface of the scaffolds using Scanning Electron Microscopy (SEM).

RESULTS AND DISCUSSION

Morphology observation and porosity measurements

The microstructural properties, including pore size, distribution, and shape, significantly influence cell infiltration, proliferation, and function in tissue engineering. The morphological characteristics of the composite scaffolds with $MgCl_2$ were examined using Scanning Electron Microscopy (SEM) images, as shown in Figure 1.

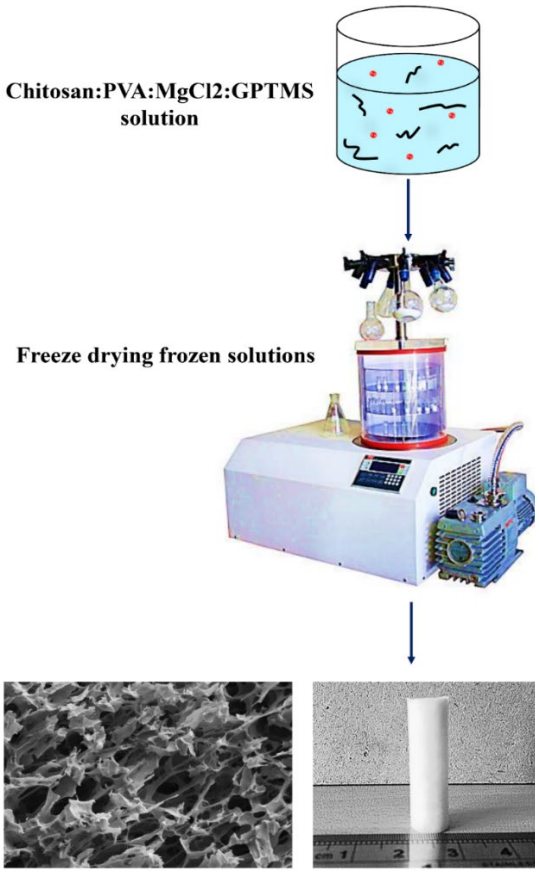

Fig. 1. Freeze drying process of prepared CPM porous scaffolds

SEM images revealed a porous structure with a three-dimensional (3D) interconnected network throughout the scaffolds across all compositions. Elongated pores were observed as the proportion of $MgCl_2$ increased. The freeze-drying technique involves freezing a suspension of polymers and $MgCl_2$, which traps the suspension between growing ice crystals, resulting in a continuous network of ice crystals surrounded by a polymeric matrix. The pore structure of the scaffold reflects the ice crystal formation during the freezing process, suggesting that the pore architecture can be controlled by modifying the freezing conditions used in freeze-drying. Freezing is the initial step in the freeze-drying process, and this stage significantly influences its overall effectiveness. The first event in freezing involves primary nucleation (heterogeneous ice nucleation), followed by secondary nucleation, which progresses to encompass portions of the liquid volume. This process stops when the liquid temperature reaches the equilibrium freezing temperature. Consequently, the addition of $MgCl_2$ lowers the freezing temperature of the suspension, allowing ice crystals to grow larger due to extended growth time. Additionally, a higher solute concentration in the solution increases the number of nucleation sites, promoting further ice crystal growth. Another factor contributing to the larger pore size in scaffolds with added $MgCl_2$ is the tendency for scaffold collapse during the freeze-drying process, which counteracts pore fusion and reduces pore size. However, due to the interaction between $MgCl_2$ and the polymer matrix, which acts as a filler, slight collapse occurs with increased $MgCl_2$ addition, leading to enlarged pores. When $MgCl_2$ is incorporated into polymer solutions at varying concentrations, the composite scaffolds exhibit a more porous structure with a broader distribution of holes and pores. Porosity measurements indicated varying pore sizes among the three samples, attributed to changes in the $MgCl_2$ ratios, as shown in Figure 2.

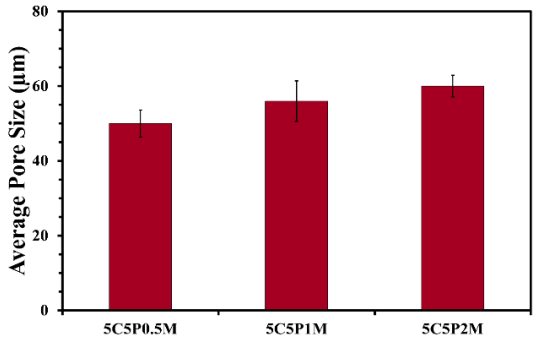

Fig. 2. Average pore size of samples, among the $MgCl_2$ added to the porous scaffolds

These differences in pore size indicate that lower $MgCl_2$ content results in smaller diameter pores and a tighter network structure in porous scaffolds. The pore size of the scaffolds increased from 50 µm to 55 µm and 60 µm for the 5C5P0.5M, 5C5P1M, and 5C5P2M scaffolds, respectively. As concluded, higher porosity in scaffolds provides more space and nutrition to cells and tissue than lower porosity, which is facilitated by an increased $MgCl_2$ ratio. Figure 2 illustrates the average pore sizes of the scaffold samples as a function of the $MgCl_2$ content incorporated into the porous structures. The data demonstrate how varying concentrations of $MgCl_2$ affect the pore architecture of the scaffolds, emphasizing the relationship between the amount of $MgCl_2$ added and the resultant pore size. As the concentration of $MgCl_2$ increases, noticeable changes in pore size and distribution are observed, indicating that $MgCl_2$ plays a crucial role in modifying the structural properties of the scaffolds. This relationship is significant for applications in tissue engineering, where optimal pore size is essential for facilitating cell infiltration, nutrient transport, and overall scaffold functionality. The results suggest that carefully manipulating $MgCl_2$ concentrations can tailor scaffold properties to meet specific biological requirements.

FTIR analyses

Figure 3 shows the FTIR spectra of chitosan, PVA, GPTMS, $MgCl_2$, and composite scaffolds. In the spectrum of pure PVA, the bands at 3440 cm^{-1} and 2921 cm^{-1} are attributed to the –OH and CH_2 stretching vibrations, respectively. The observed absorption peaks in PVA are 1734 cm^{-1} (C=O), 1150 cm^{-1} (OH), 1098 cm^{-1} (C–O), and 850 cm^{-1} (C–C). The absorption peak at 1000–1100 cm^{-1} corresponds to the stretching vibration of C–O groups in PVA. The infrared spectrum of chitosan shows peaks around 894 cm^{-1} and 1159 cm^{-1}, which are attributed to the saccharine structure. The C=O stretching vibration of amide groups (amide I) appears at 1647.26 cm^{-1}, the NH_2 bending vibration of the amino group is observed at 1585.54 cm^{-1}, the C–N stretching vibration is seen at 1386 cm^{-1}, and the NH stretching vibration occurs at 668 cm^{-1}. The hydroxyl stretching of chitosan is observed at 3353 cm^{-1}. In the FTIR spectrum of GPTMS, the following bands are observed: C–H stretching vibration at 2962.02 cm^{-1}, C–O–C stretching vibration at 1094.24 cm^{-1}, Si–O stretching vibration at 1024 cm^{-1}, Si–C stretching vibration at 1261 cm^{-1}, and oxirane ring vibration at 905 cm^{-1}. Additionally, the FTIR spectrum of the composite scaffolds (CPM)

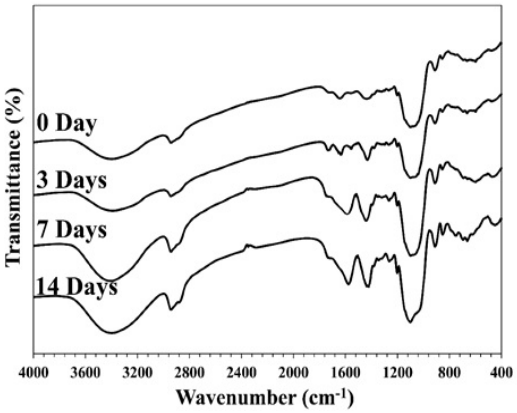

Fig. 3. FTIR spectra of chitosan, PVA, MgCl2, CPTMS and 5C5P0.M, 5C5P1M and 5C5P2M scaffolds

shows the O–H stretching vibration at 3434.48 cm^{-1}, C–H stretching vibration at 2924.18 cm^{-1}, and C=O vibrations of the amide group (amide I and amide II) at 1647.26 cm^{-1} and 1565.42 cm^{-1}, respectively, as shown in Figure 3.

The disappearance of the absorption band at 910 cm^{-1} (oxirane ring) and the shift of the NH bending absorption band from 1585.54 cm^{-1} (primary amine) to 1560.24 cm^{-1} indicate that the oxidant groups of GPTMS have reacted with the amine groups of chitosan. Additionally, the broad band around 1045 cm^{-1} is attributed to the stretching vibration of Si–O–Si groups.

Mechanical properties

The compressive strength of CPM scaffolds was shown in Figure 4. The compressive strength markedly increased when the concentration of $MgCl_2$ was increased. Increasing the amount of MgCl2 to a 1 mass ratio increased compressive strength from 0.5 MPa to 0.9 MPa. Also, further increase of $MgCl_2$ content to 2 mass ratio led to improvement in the mechanical properties of the composite scaffolds, reaching 1.9 MPa.

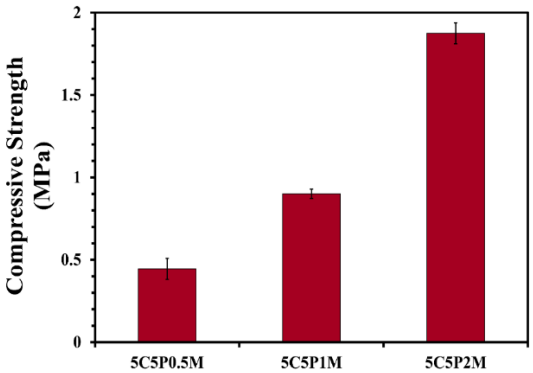

Fig. 4. Compressive strength of 5C5P0.M, 5C5P1M and 5C5P2M.

These results demonstrate the positive effects of $MgCl_2$ on the mechanical properties of the specimens. The improvement in the mechanical properties of the scaffolds can be attributed to their porosity and composition [29-32]. However, the increase in $MgCl_2$ also results in larger pores, and the dominant factor in the enhancement of compressive strength is likely the increased pore size. The enhancement of compressive strength in the samples with increased $MgCl_2$ content may be related to the role of these particles as stiff fillers within the polymer matrix, which enhances the hardness and stiffness of the composite [31-34]. Additionally, it is essential to note that the distribution of the particles in the polymer matrix plays a crucial role in achieving reasonable mechanical properties. A homogeneous distribution of particles leads to a significant improvement in mechanical properties, as demonstrated in this experiment. It was observed that due to biochemical bonding between Mg^{2+} ions and the amide (-NH) groups of chitosan, strong interactions between the filler and matrix occurred, which restrict the motion of the matrix [25-29].

Water absorption test

The capacity of a scaffold to retain water is a crucial factor in assessing cell infiltration within a three-dimensional structure. Figure 5 (a-b) presents the swelling ratios of various scaffolds. The swelling property of the 5C5P0.5 scaffold was approximately twice that of the 5C5P2M scaffold. The results indicated no significant differences in water absorption among different samples of the same scaffold over specific incubation periods. The water-binding capacity of the PVA/chitosan sample can be attributed to its inherent hydrophilicity, as evidenced by the presence of –OH groups in PVA and –OH and –NH groups in chitosan, as well as the maintenance of its three-dimensional structure.

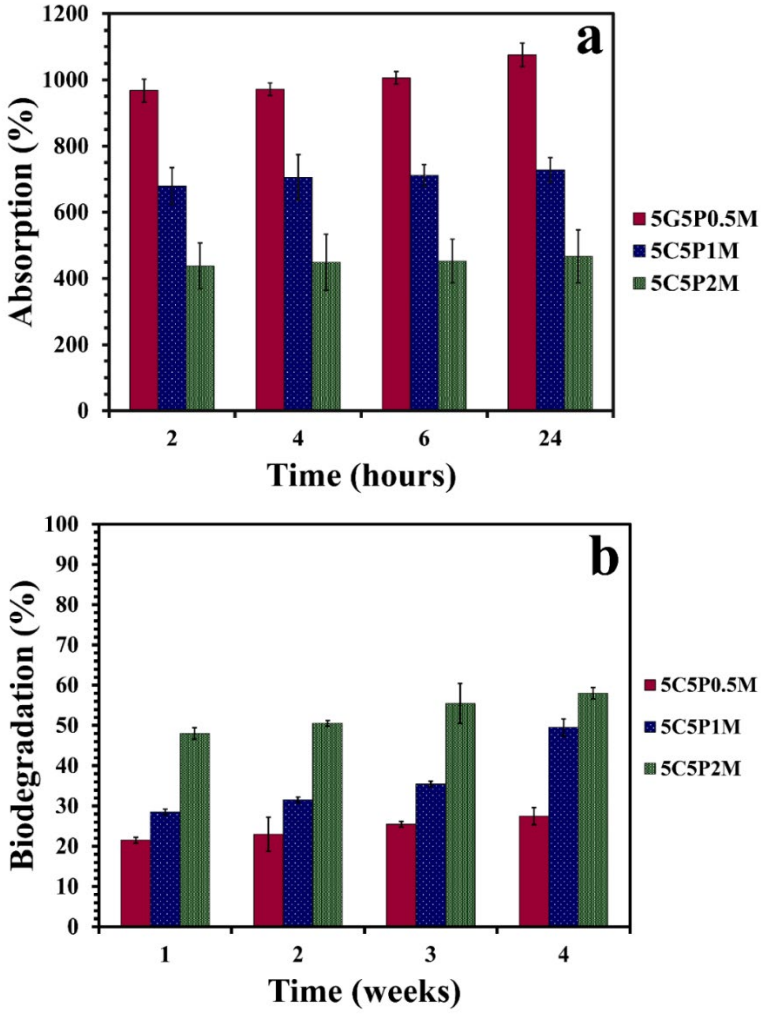

Fig. 5. Results of (a) water absorption and (b) biodegradation of the composite scaffolds.

It was observed that the swelling ratio decreased with increasing $MgCl_2$ content, likely because $MgCl_2$ reduced the hydrophilicity of the scaffolds by binding to hydrophilic groups. These findings suggest that the primary determinant of water absorption is the presence of hydrophilic groups, rather than the scaffolds' porosity (shape and size). Furthermore, although an increase in $MgCl_2$ ratio was expected to diminish the mechanical properties of the scaffolds due to reduced swelling, a similar behavior in strength and swelling among the samples demonstrated a controlled balance between the structural integrity and composition of the scaffolds, which is optimal for tissue engineering applications. Figure 5 (a-b) illustrates the degree of biodegradation of all scaffolds. The samples incubated in PBS showed weight loss and gradually degraded over varying periods. The weight loss of the 5C5P0.5M scaffold occurred very slowly, with negligible changes observed throughout the degradation period. In contrast, increasing the $MgCl_2$ content accelerated the degradation of the scaffolds in the PBS solution. For instance, after one week, the biodegradation degree for the 5C5P2M specimen was 49%, compared to only 20% for the 5C5P0.5M scaffold. These results indicate that the presence of $MgCl_2$ reduced the biostability of the scaffolds over time, with higher $MgCl_2$ concentrations correlating with greater weight loss percentages. The increased weight loss of the composite scaffolds may be attributed to the degradation of $MgCl_2$ and the subsequent release of ions into the solution. It is hypothesized that the degradation of acidic products from the polymers in the scaffolds led to the release of alkaline ions (Mg^{2+}) to counteract the acidification of the solution caused by these acidic byproducts. This buffering behavior could be advantageous for composite scaffolds, as it may help mitigate potential inflammatory responses associated with the acidic degradation of polymers. Additionally, the larger pore size resulting from $MgCl_2$ incorporation enhances the connection between the solution within the scaffold and the surrounding environment, facilitating a more rapid ionic release.

In vitro bioactivity of scaffolds in SBF

The in vitro bioactivity of the 5C5P1M scaffolds in simulated body fluid (SBF) demonstrated the biomaterials' ability to bond with living bone. The bioactivity of these scaffolds was assessed by immersing them in SBF for periods of 3, 7, and 14 days. SEM images of the scaffolds after soaking are displayed in Figure 6 (a-d). After 3 days of incubation, apatite nucleation was observed on the exposed surfaces of the scaffold; however, the apatite particles did not uniformly cover the entire composite surface. The density of spherical particles increased with extended soaking durations. These results show that the 5C5P1M scaffolds are capable of inducing the formation of hydroxyapatite (HA) particles on their surface in SBF, even during shorter immersion periods. This observation is consistent with previous research highlighting the role of magnesium in apatite formation. Furthermore, the bioactive behavior of the $MgCl_2$ scaffolds was corroborated by the Fourier-transform infrared (FTIR) spectra, as shown in Figure 6.

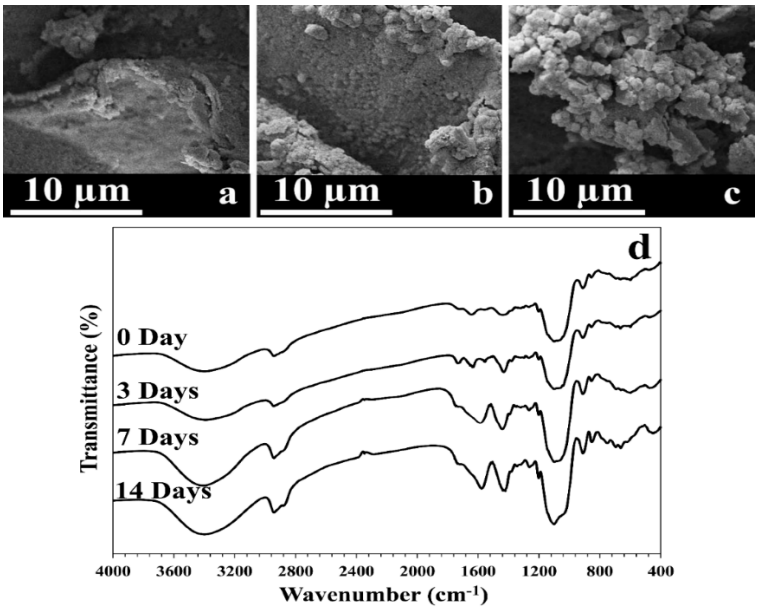

Fig. 6. SEM images of 5C5P1M scaffolds after soaking in SBF solution (a): 3 days, (b): 7 days, (c): 14 day and FTIR spectra of 5C5P1M scaffolds after different time immersion

The absorption peak at 1045 cm^{-1} was attributed to the asymmetrical stretching of PO_4^{3-}, and the peak at 603 cm^{-1} was assigned to the bending modes of PO_4^{3-} [21]. After 14 days of soaking in SBF solution, stronger peaks at 603 cm^{-1} and 1045 cm^{-1} were observed. The band at 1454 cm^{-1}, corresponding to the vibration mode of carbonate, became sharper with increasing immersion time. The PO_4^{3-} peak at 960 cm^{-1} intensified with longer immersion times [30]. The most significant increase in the PO_4^{3-} peak was observed after 14 days. A band near 460 cm^{-1}, which developed after 14 days, indicated the maturation of the HA particles [31].

Cytotoxicity and cell adhesion assay

Figure 7 (a-b) shows the absorbance obtained from an MTT assay of MG-63 osteoblast cells cultured with the extraction media of the scaffolds, in comparison with the control. After 3 days, the average absorbance intensity of the 5C5P1M scaffolds was 0.8, which markedly increased to 0.25 after 5 days. The results indicated that after 3 and 5 days, the number of cells surpassed the number of initially seeded cells, and MG-63 cells continued proliferating on the scaffolds. The results demonstrated that the prepared scaffolds were non-toxic to MG-63 osteoblast cells and promising candidates for porous tissue scaffolds.

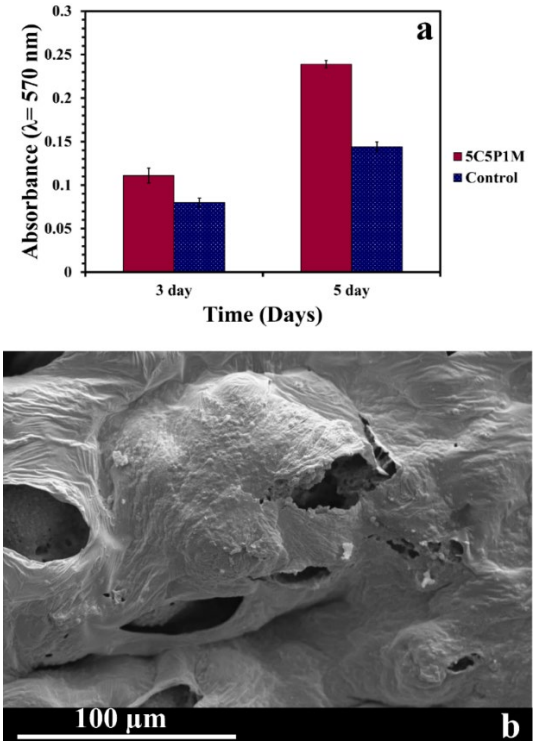

Fig. 7. a) Formazan absorption in MTT assays MG-63osteoblast cells seeded on the samples, and b) SEM images of MG-63cells seeded on osteoblast cells after 48 h

As shown in Figure 7 (b), the SEM images of the cells cultured on the 5C5P1M scaffolds for 2 days demonstrate that the MG-63 cells interacted with the scaffold, forming a continuous layer. The improvement in cell adhesion by adding $MgCl_2$ is attributed to the formation of more silanol groups on the scaffold surface, which results in enhanced cell adhesion [35-38]. The present study has several limitations that should be addressed in future research. Firstly, while the in vitro experiments provide valuable insights into the scaffold's properties and biocompatibility, in vivo studies are necessary to evaluate the scaffold's performance in a physiologically relevant environment. The interaction between the scaffold, host tissue, and the immune system should be investigated to ensure the long-term success of the implant. Additionally, although the study demonstrated the positive effects of $MgCl_2$ on the scaffold's properties, the optimal concentration of $MgCl_2$ was not fully explored. Other bioactive agents could further enhance the scaffold's functionality and clinical relevance [39-44]. Future studies should also focus on the scale-up and manufacturing processes for these scaffolds to ensure consistent quality and reproducibility, as well as the integration of the scaffolds with other tissue engineering strategies, such as the use of stem cells or the incorporation of vascularization cues, to develop more comprehensive bone regeneration solutions [45-46]. Numerous contributions in nanomedicine and tissue engineering have led to innovative applications, including the development of three-dimensional printed electroconductive scaffolds for bone cancer therapy, the use of artificial intelligence to assess bioceramics combined with magnetite bio-nanocomposites for hyperthermia, and the examination of lithium disilicate ceramics reinforced with titanium nanoparticles to enhance the durability of dental materials. These efforts collectively advance the integration of nanotechnology and bioengineering to improve therapeutic strategies and patient outcomes [47-55].

CONCLUSION

Novel porous composite scaffolds incorporating chitosan, PVA, GPTMS, and $MgCl_2$ particles were fabricated using a freeze-drying method, and the influence of $MgCl_2$ on their properties was assessed. The inclusion of $MgCl_2$ in the polymer matrix resulted in scaffolds with increased porosity and compressive strength compared to the unmodified scaffolds. Furthermore, the bioactivity of the 5C5P1M scaffolds improved with extended immersion time. Our results indicate that adding

$MgCl_2$ decreased the swelling ratio while enhancing biodegradation. In vitro cytotoxicity and cell proliferation tests demonstrated that the composite scaffolds were non-cytotoxic, promoting better cell adhesion and proliferation on their surfaces. It is proposed that these composite scaffolds could serve as effective templates for bone tissue engineering applications. In conclusion, this study successfully developed a novel porous composite scaffold composed of chitosan, polyvinyl alcohol, GPTMS, and $MgCl_2$ using the freeze-drying technique. Incorporating $MgCl_2$ significantly improved the scaffolds' mechanical properties, bioactivity, and biodegradation, making them promising candidates for bone tissue engineering applications. The scaffolds also exhibited excellent biocompatibility and supported the proliferation of MG-63 osteoblast cells. While the in vitro results are promising, further in vivo investigations are necessary to fully evaluate the scaffold's performance and potential for clinical translation. Additionally, optimizing the $MgCl_2$ content and exploring the integration of other bioactive agents could enhance scaffold functionality and clinical relevance.

ACKNOWLEDGEMENTS

None

CONFLICT OF INTEREST

No conflict of interest was declared.

FUNDING

None

REFERENCES

1. Nie L, Chen D, Suo J, Zou P, Feng S, Yang Q, et al. Physicochemical characterization and biocompatibility in vitro of biphasic calcium phsphate/polyvinyl alcohol scaffolds prepared by freeze-drying method for bone tissue engineering applications. Colloids Surf B Biointerfaces. 2012;100:169-176.
2. Diba M, Kharaziha M, Fathi M, Gholipourmalekabadi M, Samadikuchaksaraei A. Preparation and characterization of polycaprolactone/forsterite nanocomposite porous scaffolds designed for bone tissue regeneration. Compos Sci Technol. 2012;72:716-723.
3. Ma L, Gao C, Mao Z, Zhou J, Shen J, Hu X, et al. Collagen/chitosan porous scaffolds with improved biostability for skin tissue engineering. Biomaterials. 2003;24:4833-4841.
4. Sowjanya J, Singh J, Mohita T, Sarvanan S, Moorthi A, Srinivasan N, et al. Biocomposite scaffolds containing chitosan/alginate/nano-silica for bone tissue engineering. Colloids Surf B Biointerfaces. 2013;109:294-300.
5. Levengood SKL, Zhang M. Chitosan-based scaffolds for bone tissue engineering. J Mater Chem B. 2014;2:3161-184.
6. Jasemi, A., Moghadas, B. K., Khandan, A., & Saber-Samandari, S. A porous calcium-zirconia scaffolds composed of magnetic nanoparticles for bone cancer treatment: Fabrication, characterization and FEM analysis. Cer Int. 2022; 48(1), 1314-1325.
7. Tonda-Turo C, Gentile P, Saracino S, Chiono V, Nandagiri VK, Muzio G, et al. Comparative analysis of gelatin scaffolds crosslinked by genipin and silane coupling agent. Int J Biol Macromol. 2011;49:700-706.
8. Salmani, M. M., Hashemian, M., & Khandan, A. Therapeutic effect of magnetic nanoparticles on calcium silicate bioceramic in alternating field for biomedical application. Cer Int. 2020; 46(17), 27299-27307.
9. Pandis C, Madeira S, Matos J, Kyritsis A, Mano JF, Ribelles JLG. Chitosan–silica hybrid porous membranes. Mater Sci Eng C. 2014;42:553-561.
10. Croisier F, Jérôme C. Chitosan-based biomaterials for tissue engineering. Eur Polym J. 2013;49:780-92.
11. Kadir M, Aspanut Z, Majid S, Arof A. FTIR studies of plasticized poly (vinyl alcohol)–chitosan blend doped with NH4NO3 polymer electrolyte membrane. Spectrochim Acta A Mol Biomol Spectrosc. 2011;78:1068-1074.
12. Guo R, Hu C, Pan F, Wu H, Jiang Z. PVA–GPTMS/TEOS hybrid pervaporation membrane for dehydration of ethylene glycol aqueous solution. J Membr Sci. 2006;281:454-462.
13. Peng F, Lu L, Sun H, Wang Y, Wu H, Jiang Z. Correlations between free volume characteristics and pervaporation permeability of novel PVA–GPTMS hybrid membranes. J Membr Sci. 2006;275:97-104.
14. Kanimozhi K, Basha SK, Kumari VS. Processing and characterization of chitosan/PVA and methylcellulose porous scaffolds for tissue engineering. Mater Sci Eng C. 2016;61:484-91.
15. Agrawal P, Pramanik K. Chitosan-poly (vinyl alcohol) nanofibers by free surface electrospinning for tissue engineering applications. Tissue Eng Regen Med. 2016;13:485-497.
16. Shirosaki Y, Okayama T, Tsuru K, Hayakawa S, Osaka A. In vitro bioactivity and MG63 cytocompatibility of chitosan-silicate hybrids. Int J Mater Chem. 2013;3:1-7.
17. Ding S, Zhang J, Tian Y, Huang B, Yuan Y, Liu C. Magnesium modification up-regulates the bioactivity of bone morphogenetic protein-2 upon calcium phosphate cement via enhanced BMP receptor recognition and Smad signaling pathway. Colloids Surf B Biointerfaces. 2016;145:140-151.
18. Huang B, Yuan Y, Li T, Ding S, Zhang W, Gu Y, et al. Facilitated receptor-recognition and enhanced bioactivity of bone morphogenetic protein-2 on magnesium-substituted hydroxyapatite surface. Sci Rep. 2016;6.
19. Foroutan S, Hashemian M, Khandan, AS. A novel porous graphene scaffold prepared using freeze-drying technique for orthopedic approaches:

fabrication and buckling simulation using GDQ method. Iran J Mater Sci Eng. 2020; 17(4).
20. Huan Z, Leeflang S, Zhou J, Zhai W, Chang J, Duszczyk J. In vitro degradation behavior and bioactivity of magnesium-Bioglass® composites for orthopedic applications. J Biomed Mater Res B Appl Biomater. 2012;100:437-446.
21. Kheradmandfard M, Fathi M, Ahangarian M, Zahrani EM. In vitro bioactivity evaluation of magnesium-substituted fluorapatite nanopowders. Ceram Int. 2012;38:169-175.
22. Tang XC, Pikal MJ. Design of freeze-drying processes for pharmaceuticals: practical advice. Pharm Res. 2004;21:191-200.
23. Searles JA, Carpenter JF, Randolph TW. The ice nucleation temperature determines the primary drying rate of lyophilization for samples frozen on a temperature-controlled shelf. J Pharm Sci. 2001;90:860-871.
24. Haugh MG, Murphy CM, O'Brien FJ. Novel freeze-drying methods to produce a range of collagen–glycosaminoglycan scaffolds with tailored mean pore sizes. Tissue Eng Part C Methods. 2009;16:887-984.
25. Wu H, Tao Z, Gao P, Chen GH. Ice crystal sizes and their impact on microwave assisted freeze drying. Chin J Chem Eng. 2004;12:831-835.
26. Kumar A, Negi YS, Choudhary V, Bhardwaj NK. Microstructural and mechanical properties of porous biocomposite scaffolds based on polyvinyl alcohol, nano-hydroxyapatite and cellulose nanocrystals. Cellulose. 2014;21:3409-3426.
27. Cziczo D, Abbatt J. Infrared observations of the response of NaCl, MgCl2, NH4HSO4, and NH4NO3 aerosols to changes in relative humidity from 298 to 238 K. J Phys Chem A. 2000;104:2038-2047.
28. Sule-Suso J, Forster A, Zholobenko V, Stone N, El Haj A. Effects of CaCl2 and MgCl2 on Fourier transform infrared spectra of lung cancer cells. Appl Spectrosc. 2004;58:61-67.
29. Wei J, Chen F, Shin JW, Hong H, Dai C, Su J, et al. Preparation and characterization of bioactive mesoporous wollastonite–polycaprolactone composite scaffold. Biomaterials. 2009;30:1080-1088.
30. Kiani A, Hanna JV, King SP, Rees GJ, Smith ME, Roohpour N, et al. Structural characterization and physical properties of P2O5–CaO–Na2O–TiO2 glasses by Fourier transform infrared, Raman and solid-state magic angle spinning nuclear magnetic resonance spectroscopies. Acta Biomater. 82012;8:333-340.
31. Clupper DC, Gough JE, Embanga PM, Notingher I, Hench LL, Hall MM. Bioactive evaluation of 45S5 bioactive glass fibres and preliminary study of human osteoblast attachment. J Mater Sci Mater Med. 2004;15:803-808.
32. Liang H, Mirinejad MS, Asefnejad A, Baharifar H, Li X, Saber-Samandari S, et al. Fabrication of tragacanthin gum-carboxymethyl chitosan bio-nanocomposite wound dressing with silver-titanium nanoparticles using freeze-drying method. Mater Chem Phys. 2022;279:125770.
33. Karimi M, Asefnejad A, Aflaki D, Surendar A, Baharifar H, Saber-Samandari S, et al. Fabrication of shapeless scaffolds reinforced with baghdadite-magnetite nanoparticles using a 3D printer and freeze-drying technique. J Mater Res Technol. 2021;14:3070-9.
34. Foroutan S, Hashemian M, Khosravi M, Nejad MG, Asefnejad A, Saber-Samandari S, Khandan A. A porous sodium alginate-CaSiO3 polymer reinforced with graphene nanosheet: fabrication and optimality analysis. Fibers Polym. 2021;22:540-549.
35. Raisi A, Asefnejad A, Shahali M, Doozandeh Z, Kamyab Moghadas B, Saber-Samandari S, Khandan A. A soft tissue fabricated using a freeze-drying technique with carboxymethyl chitosan and nanoparticles for promoting effects on wound healing. J Nanoanalysis. 2020;7(4):262-274.
36. Iranmanesh P, Ehsani A, Khademi A, Asefnejad A, Shahriari S, Soleimani M, Khandan A. Application of 3D bioprinters for dental pulp regeneration and tissue engineering (porous architecture). Transp Porous Media. 2022;142(1):265-293.
37. Jamnezhad S, Asefnejad A, Motififard M, Yazdekhasti H, Kolooshani A, Saber-Samandari S, Khandan A. Development and investigation of novel alginate-hyaluronic acid bone fillers using freeze drying technique for orthopedic field. Nanomed Res J. 2020;5(4):306-315.
38. Raisi A, Asefnejad A, Shahali M, Sadat Kazerouni ZA, Kolooshani A, Saber-Samandari S, Khandan A. Preparation, characterization, and antibacterial studies of N,O-carboxymethyl chitosan as a wound dressing for bedsore application. Arch Trauma Res. 2020;9(4):181-188.
39. Li X, Saeed SS, Beni MH, Morovvati MR, Angili SN, Toghraie D, et al. Experimental measurement and simulation of mechanical strength and biological behavior of porous bony scaffold coated with alginate-hydroxyapatite for femoral applications. Compos Sci Technol. 2021;214:108973.
40. Moarrefzadeh A, Morovvati MR, Angili SN, Smaisim GF, Khandan A, Toghraie D. Fabrication and finite element simulation of 3D printed poly L-lactic acid scaffolds coated with alginate/carbon nanotubes for bone engineering applications. Int J Biol Macromol. 2023;224:1496-1508.
41. Khandan A, Nassireslami E, Saber-Samandari S, Arabi N. Fabrication and characterization of porous bioceramic-magnetite biocomposite for maxillofacial fractures application. Dent Hypotheses. 2020;11(3):74-85.
42. Khandan A, Karamian E, Bonakdarchian M. Mechanochemical synthesis evaluation of nanocrystalline bone-derived bioceramic powder using for bone tissue engineering. Dent Hypotheses. 2014;5(4):155-161.
43. Attaeyan A, Shahgholi M, Khandan A. Fabrication and characterization of novel 3D porous Titanium-6Al-4V scaffold for orthopedic application using selective laser melting technique. Iran J Chem Chem Eng. (IJCCE). 2024;43(1).
44. Khademi A, Khandan A, Iranmanesh P, Heydari M. Development of a 3D bioprinted alginate-gelatin

hydrogel scaffold loaded with calcium phosphates for dental pulp tissue regeneration. Iran J Chem Chem Eng. 2025; 44(01): 1-16.
45. Safaei MM, Abedinzadeh R, Khandan A, Barbaz-Isfahani R, Toghraie D. Synergistic effect of graphene nanosheets and copper oxide nanoparticles on mechanical and thermal properties of composites: Experimental and simulation investigations. Mater Sci Eng B. 2023;289:116248.
46. Khandan A, Khosravi M, Roustazadeh D, Aghadavoudi F. Impact of alumina and carbon nanotubes on mechanical properties of a composite: molecular dynamic (MD) simulation. Iran J Chem Chem Eng. 2024; 43 (8): 2866-2877.
47. Monshi M, Esmaeili S, Kolooshani A, Moghadas BK, Saber-Samandari S, Khandan A. A novel three-dimensional printing of electroconductive scaffolds for bone cancer therapy application. Nanomed J. 2020;7(2).
48. Montazeran AH, Saber Samandari S, Khandan A. Artificial intelligence investigation of three silicates bioceramics-magnetite bio-nanocomposite: hyperthermia and biomedical applications. Nanomed J. 2018;5(3):163-171.
49. Rajaei A, Kazemian M, Khandan A. Investigation of mechanical stability of lithium disilicate ceramic reinforced with titanium nanoparticles. Nanomed Res J. 2022;7(4):350-359.
50. Yekta HJ, Shahali M, Khorshidi S, Rezaei S, Montazeran AH, Samandari SS, Khandan A. Mathematically and experimentally defined porous bone scaffold produced for bone substitute application. Nanomed J. 2018;5(4).
51. Jafaripour N, Omidvar H, Saber-Samandari S, Mohammadi R, Shokrani Foroushani R, Kamyab Moghadas B, Khandan A. Synthesize and Characterization of a Novel Cadmium Selenide Nanoparticle with Iron Precursor Applicable in Hyperthermia of Cancer Cells. Int J Nanoscience Nanotechnology. 2021;17(2):77-90.
52. Salimi K, Eghbali S, Jasemi A, Shokrani Foroushani R, Joneidi Yekta H, Latifi M, Khandan A. An artificial soft tissue made of nano-alginate polymer using bioxfab 3D bioprinter for treatment of injuries. Nanochemistry Res. 2020;5(2):120-127.
53. Fatalla AA, Arzani S, Veseli E, Khademi A, Khandan A, Fahmy MD, Kelishadi R. Revolutionizing systematic reviews and meta-analyses: the role of artificial intelligence in evidence synthesis. Dent Hypotheses. 2023;14(4):93-94.
54. Mirmohammadi H, Kolahi J, Khandan A. Bibliometric analysis of dental preprints published in 2022. Dent Hypotheses. 2023;14(1):1-2.
55. Khandan A, Ozada N, Karamian E. Novel microstructure mechanical activated nano composites for tissue engineering applications. J Bioeng Biomed Sci. 2015;5(1):1.